Environmental Science & Technology

Article

Cite This: Environ. Sci. Technol. 2018, 52, 12316−12326

pubs.acs.org/est

Impact of Organic Matter on Iron(II)-Catalyzed Mineral Transformations in Ferrihydrite−Organic Matter Coprecipitates

Laurel K. ThomasArrigo,*[,†] James M. Byrne,[‡] Andreas Kappler,[‡] and Ruben Kretzschmar[†]

[†]Soil Chemistry Group, Institute of Biogeochemistry and Pollutant Dynamics, Department of Environmental Systems Science, ETH Zurich, Universitätstrasse 16, CHN, CH-8092 Zurich, Switzerland

[‡]Geomicrobiology Group, Centre for Applied Geosciences (ZAG), University of Tübingen, Sigwartstrasse 10, D-72076 Tübingen, Germany

Supporting Information

ABSTRACT: Poorly crystalline Fe(III) (oxyhydr)oxides like ferrihydrite are abundant in soils and sediments and are often associated with organic matter (OM) in the form of mineral-organic aggregates. Under anoxic conditions, interactions between aqueous Fe(II) and ferrihydrite lead to the formation of crystalline secondary minerals, like lepidocrocite, goethite, or magnetite. However, the extent to which Fe(II)-catalyzed mineral transformations are influenced by ferrihydrite-associated OM is not well understood. We therefore reacted ferrihydrite-PGA coprecipitates (PGA = polygalacturonic acid, C:Fe molar ratios = 0−2.5) and natural Fe-rich organic flocs (C:Fe molar ratio = 2.2) with 0.5−5.0 mM isotopically labeled ^{57}Fe(II) at pH 7 for 5 weeks. Relying on the combination of stable Fe isotope tracers, a novel application of the PONKCS method to Rietveld fitting of X-ray diffraction (XRD) patterns, and ^{57}Fe Mössbauer spectroscopy, we sought to follow the temporal evolution in Fe mineralogy and elucidate the fate of adsorbed ^{57}Fe(II). At low C:Fe molar ratios (0−0.05), rapid oxidation of surface-adsorbed ^{57}Fe(II) resulted in ^{57}Fe-enriched crystalline minerals and nearly complete mineral transformation within days. With increasing OM content, the atom exchange between the added aqueous ^{57}Fe(II) and Fe in the organic-rich solids still occurred; however, XRD analysis showed that crystalline mineral precipitation was strongly inhibited. For high OM-content materials (C:Fe ≥ 1.2), Mössbauer spectroscopy revealed up to 39% lepidocrocite in the final Fe(II)-reacted samples. Because lepidocrocite was not detectable by XRD, we suggest that the Mössbauer-detected lepidocrocite consisted of nanosized clusters with lepidocrocite-like local structure, similar to the lepidocrocite found in natural flocs. Collectively, our results demonstrate that the C content of ferrihydrite−OM coprecipitates strongly impacts the degree and pathways of Fe mineral transformations and iron atom exchange during reactions with aqueous Fe(II).

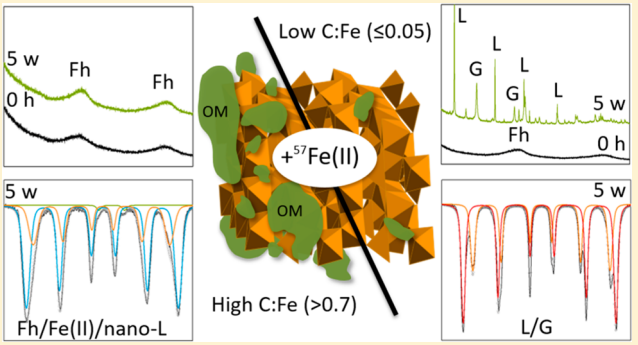

INTRODUCTION

Iron(III) oxides and oxyhydroxides, herein collectively termed Fe(III) (oxyhydr)oxides, are among the most important and reactive components of soils, sediments, and aquatic environments, influencing nutrient cycling and contaminant mobility.[1,2] In nature, Fe(III) (oxyhydr)oxides often form in the presence of dissolved organic matter (OM), resulting in mineral-organic associations.[2−10] Coprecipitation of Fe(III) (oxyhydr)oxides in the presence of dissolved OM results in the preferential uptake of aromatic-rich compounds found in terrestrially derived OM.[11−17] In contrast, biogenic Fe(III) (oxyhydr)oxides, formed via microaerophilic, anoxygenic phototrophic, or nitrate-reducing Fe(II)-oxidizing bacteria, tend to incorporate cellular-derived OM rich in carboxylic and aliphatic acids.[18−21] Occlusion of organic C within the mineral-organic aggregate structure or micropore space and the stability of the chemical bonds between OM and the Fe(III) mineral surface prevents biodegradation and mineralization of C. Thus, OM-associated Fe(III) (oxyhydr)oxides are recognized as critically important to the long-term stabilization of organic C in soils and marine sediments.[7,22−25]

In permanently or recurrently anoxic environments, mineral-organic aggregates may endure rapid changes in the prevailing redox conditions. Exposure to abiotic or microbially derived ferrous Fe (Fe(II)) triggers mineral recrystallization and transformation processes in Fe(III) (oxyhydr)oxides, often promoting Fe mineral transformation toward thermodynamically stable mineral phases. This may occur via iron atom exchange, where adsorption of aqueous Fe(II) onto the Fe(III) (oxyhydr)oxides leads to the immediate oxidation of the surface-adsorbed Fe(II), the transfer of electrons to structural

Received: June 12, 2018
Revised: September 28, 2018
Accepted: October 1, 2018
Published: October 16, 2018

DOI: 10.1021/acs.est.8b03206
Environ. Sci. Technol. 2018, 52, 12316−12326

Fe(III), and the release of structural Fe(III) from a spatially distinct location as Fe(II).[26−28] Most dramatic are the reactions between aqueous Fe(II) and ferrihydrite (Fh) ($Fe_{10}O_{14}(OH)_2$ + mH_2O), a poorly crystalline Fe(III) oxyhydroxide which, in nature, is often first to form upon oxidation of ferrous Fe in solution.[29] Fe(II)-catalyzed transformations of Fh can result in goethite (α-FeOOH), lepidocrocite (γ-FeOOH), or magnetite (Fe_3O_4), with minor differences in pH, background ligands, and Fe(II):Fe(III) ratios impacting both reaction kinetics and end-phase minerals.[28,30−35] The presence of adsorbed or coprecipitated OM may also be influential.[34,36−38] Coprecipitation with OM changes aggregate structure, altering the mineral susceptibility toward microbial reduction[39,40] and ligand-controlled dissolution.[41] In addition, quinone moieties in natural OM can shuttle electrons;[42] facilitating dissimilatory reduction of Fe(III) in Fh−OM coprecipitates and promoting the release of associated C.[43,44]

In contrast to pure Fh, OM-associated Fh shows limited secondary mineral formation upon exposure to aqueous Fe(II), suggesting that OM may act to stabilize poorly crystalline Fe(III) (oxyhydr)oxides under reducing conditions.[34,36−38] In a recent study, Chen et al.[36] reacted Fh−OM coprecipitates (C:Fe molar ratios 0−1.6) with 0.2 or 2.0 mM Fe(II) for 90 days, reporting a linear correlation between increasing C content and rates of Fh preservation. However, the mechanism explaining this stabilizing effect remained unclear.[36] At higher C:Fe molar ratios (≥2.8), mineral surface sites and pores of Fh−OM coprecipitates may be completely blocked, thus preventing Fe(II) adsorption onto the mineral surface.[12] Alternatively, carboxyl or carboxy-phenolic moieties of the OM fraction may support the complexation of Fe(II) with the OM fraction,[45,46] thus limiting Fe(II) interactions with the mineral surface. Evidence for the latter was established in our previous study, where the effect of isotopically enriched ^{57}Fe(II) on Fe mineralogy was examined in naturally occurring Fe-rich organic flocs (C:Fe molar ratio = 2.2),[6] a synthetic Fh−OM coprecipitate (C:Fe molar ratio = 2.5), and a pure Fh over 7 days.[34] Mössbauer spectra of these ^{57}Fe(II)-reacted samples indicated the presence of solid-phase associated Fe(II) in all OM-containing samples.[34] Not matching common Fe(II) mineral phases[47−49] and also not observed in the pure Fh treatment, it was postulated that the solid-phase Fe(II) was likely adsorbed or complexed with the OM fraction.[34]

Additionally, time-resolved aqueous Fe isotope data indicated that varying $Fe(II)_{spike}$ concentrations and OM content could significantly alter the secondary mineral formation pathways within <1 week;[34] time scales which are relevant to environments with rapidly fluctuating redox cycles, such as wetlands or sediments. However, complementary time-resolved solid-phase mineral analyses were lacking, thus the impact of aqueous Fe(II) and OM on Fh mineral transformation pathways could not be comprehensively addressed. Therefore, in the current study, ^{57}Fe(II) was again used as a stable isotope tracer in combination with ^{57}Fe Mössbauer spectroscopy and a novel application of the PONKCS (partial or no known crystal structure) method[50] to Rietveld fitting of X-ray diffraction (XRD) patterns to investigate the fate of adsorbing ^{57}Fe(II) in relation to the rapid temporal evolution of Fe mineralogy during Fe(II)-catalyzed mineral transformations in Fh−PGA coprecipitates and a natural Fe-rich, organic floc. By including a series of Fh−OM coprecipitates of varying C:Fe molar ratios (0−2.5) and flocs from the naturally As-enriched peatland *Gola di Lago* (Switzerland, Floc 5S, C:Fe molar ratio = 2.2)[34,51] exposed to a range of $Fe(II)_{spike}$ concentrations (0.5−5.0 mM), we aimed to systematically (i) explore controls on the extent to which coprecipitated OM impedes mineral transformations in poorly crystalline Fe(III) (oxyhydr)oxides and to (ii) elucidate the fate of adsorbed Fe(II) in the presence of mineral-organic aggregates under prolonged anoxic conditions.

MATERIALS AND METHODS

Fh and Coprecipitate Synthesis and Floc Sampling. To assess the extent to which OM impacts the Fe(II)-catalyzed transformation of Fh, reaction kinetics and transformation products of a pure Fh were compared to those of Fh−OM coprecipitates of varying C:Fe molar ratios (Fh-PGA_C:Fe; PGA = polygalacturonic acid, C:Fe = 0.05, 0.7, 1.2, or 2.5) and a natural floc sample (Floc 5S).[34,51] The synthesis of Fh and the Fh−PGA coprecipitates and the floc sampling procedure are detailed in the Supporting Information. Briefly, the final C:Fe molar ratios of the synthetic Fh−PGA coprecipitates were 0.05 ± 0.01, 0.7 ± 0.0, 1.2 ± 0.0, and 2.5 ± 0.3 (n = 2, $\bar{x}$ ± σ, Table S1), hereafter named Fh−PGA_0.05, Fh−PGA_0.7, Fh−PGA_1.2, and Fh−PGA_2.5, respectively. The C:Fe molar ratio of Floc 5S was 2.2, with Fe minerals composed of Fh and lepidocrocite (ca. 50% of each).[34,51] The floc sample contained an additional 1.28 mg/g As bound in bidentate, binuclear (bridging) surface complexes with floc Fe(III) minerals.[6,51] However, due to the low As:Fe molar ratios, surface-adsorbed As was not expected to hinder Fe(II)-catalyzed mineral transformations.[52,53]

^{57}Fe(II) Isotope Tracer Experiment Setup. ^{57}Fe(II) was used as a stable isotope tracer to explore Fe(II)-catalyzed mineral transformations and the evolution of Fe isotope composition of solid- and aqueous-phase Fe in (co)precipitates and freshwater flocs. Triplicate experiments were conducted in a glovebox (N_2 atmosphere, <1 ppm (v/v) O_2), where all glassware and solutions were equilibrated for >2 days to remove trace O_2. A ^{57}Fe-enriched stock solution of 1 M Fe(II) was prepared by dissolving ^{57}Fe metal powder (95.08% ^{57}Fe, Isoflex, USA) in 2 M HCl at 70 °C overnight, which was then purged with $N_2(g)$, sealed, transferred into the glovebox, and diluted with anoxic DDI water to obtain a 100 mM ^{57}Fe(II) solution in 0.2 M HCl. The Fe concentration of the ^{57}Fe(II) solution was determined in 0.22-μm nylon filtrates photometrically with UV−vis spectrophotometry via the 1,10-phenanthroline method[54] (λ = 510 nm, Cary 60 UV−vis, Agilent). $^{57}Iron(II)_{spike}$ reactions were conducted in 50 mL glass serum bottles wrapped in Al foil. Dried sample material was weighed into each bottle and equilibrated for 12 h in ∼45 mL of anoxic 50 mM 3-(*N*-morpholino)propanesulfonic acid (MOPS) buffer adjusted to pH 7. In order to obtain equivalent solid-phase Fe concentrations in each bottle (10 mmol Fe(III)/L), the solid to solution ratios ranged from 1.01 to 1.78 g/L (Table S2). Immediately prior to starting the reactions, serum bottles were counter-spiked with aliquots of 1 M NaOH (<500 μL) to maintain a stable pH. Directly afterward, 0.22-μm filtered aliquots of the ^{57}Fe(II) stock solution were added to the bottles to obtain final $Fe(II)_{spike}$ concentrations of 0.5, 1.0, or 5.0 mM (Table S2). No additional pH adjustments were required, and pH remained at 7.0 ± 0.1 for the duration of the experiment. Serum bottles were capped with butyl rubber stoppers and placed on a horizontal shaker (250 rpm) at room temperature (24 ± 1 °C)

DOI: 10.1021/acs.est.8b03206
Environ. Sci. Technol. 2018, 52, 12316−12326

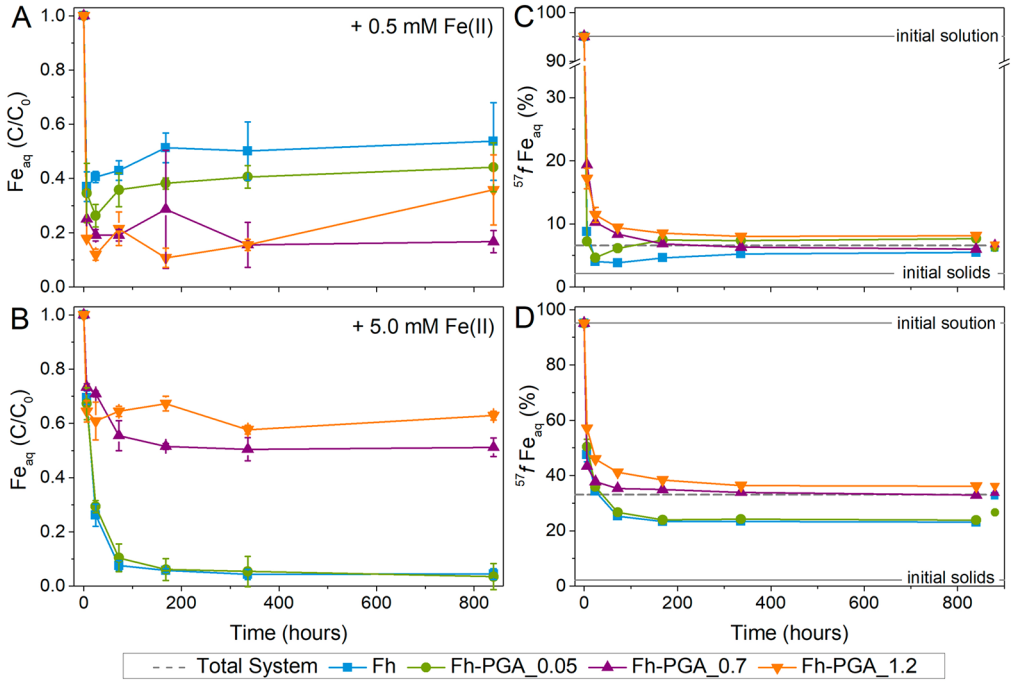

Figure 1. (A, B) Trends in dissolved Fe(II) relative to the initial $Fe(II)_{spike}$ determined in 0.22-μm filtrates for select samples reacted with 0.5 and 5.0 mM Fe(II). (C, D) Corresponding temporal changes in $f^{57}Fe_{aq}$ and the fraction of ^{57}Fe in solution. The $f^{57}Fe$ in the solid-phase after the 5 week reaction is indicated by the corresponding complementary symbols on the right. The $f^{57}Fe$ in the initial $^{57}Fe(II)_{spike}$ solution and in the initial solid-phase are shown as gray solid lines, while the calculated isotope composition of the total system is shown as a gray-dashed line. Error bars represent the standard deviation from triplicate experiments. Additional data for the remaining samples are found it the Supporting Information, Figure S5. Abbreviations: Fh = ferrihydrite, PGA = polygalacturonic acid.

for 5 weeks. Iron(II)-free controls were included for each treatment to quantify element releases originating from solid-phase dissolution.

Total Aqueous Concentrations and Fe_{aq} Speciation. Total aqueous Fe (Fe_{aq}) concentrations and speciation were determined in 0.22-μm nylon filtrates photometrically as described above.[54] In addition, for Floc 5S, total aqueous As (As_{aq}) concentrations were determined with inductively coupled plasma-mass spectrometry (ICP-MS, Agilent 8800 Triple Quad).

Iron Isotopes as Tracers. Iron isotope compositions were also determined via ICP-MS. All samples for isotope analysis were diluted to ~30 μg/L Fe and measured in a reaction cell mode with $H_2(g)$ at a flow rate of 7 mL/min to remove argide polyatomic interferences. Interferences from ^{58}Ni were accounted for through monitoring ^{60}Ni counts, though they were found to be negligible. Iron isotope mole fractions (f) were calculated by dividing the counts per second (cps) of the Fe isotope n by the sum of the total Fe isotope's cps:

$$\frac{^{n}\text{cps}}{^{54}\text{cps} + ^{56}\text{cps} + ^{57}\text{cps} + ^{58}\text{cps}} \times 100 = f^{n}\text{Fe}\ (\%) \quad (1)$$

The accuracy of this method has been previously established.[34] The reproducibility of $f^{57}Fe$ measurements was better than ±0.06% (2SD, n = 6).

The use of stable Fe isotopes enabled the investigation of iron atom exchange between Fe(III) minerals and Fe_{aq}. In this study, synthetic (co)precipitates containing natural Fe isotope abundances ($f^{54}Fe$, ~ 5.85%; $f^{56}Fe$, ~ 91.75%; $f^{57}Fe$, ~ 2.12%; and $f^{58}Fe$, ~ 0.28%)[34,55] were reacted with a highly ^{57}Fe-enriched Fe(II) solution ($f^{54}Fe$, 0.05%; $f^{56}Fe$, 3.01%; $f^{57}Fe$, 95.08%; and $f^{58}Fe$, 1.86%). Because the $Fe(II)_{spike}$ consisted primarily of ^{57}Fe (95.08%), the Fe isotope composition was discussed in terms of $f^{57}Fe$. The calculation of the isotopic composition of the total system is presented in Table S3.

Solid-Phase Sampling and Characterization. Material for solid-phase analyses was collected on 0.45-μm cellulose filters and thoroughly rinsed with anoxic DDI water. The filter residues were covered and dried in the glovebox atmosphere. Triplicate samples were combined, homogenized with a mortar and pestle, and stored in darkness until further analyses. Total Fe contents and Fe isotopic composition of (co)precipitates were determined in "initial" and "end" samples (0 and 840 h, respectively). For these analyses, ~2 mg of (un)reacted (co)precipitates were dissolved in 1 mL of 30% HCl (Ultrapur, Merck), while (un)reacted flocs were dissolved with microwave-assisted acid digestion (MLS turboWAVE). Total Fe was measured using inductively coupled plasma-optical emission spectrometry (ICP-OES, Agilent 5100), and Fe isotope composition of the dissolved solid-phase was determined with ICP-MS as described above. Total C contents of (co)precipitates and flocs were analyzed with an elemental analyzer (CHNS-932, LECO; n = 2).

Quantitative mineral-phase analyses were performed by powder X-ray diffraction (XRD, D8 Advance, Bruker) with Rietveld analysis. The dried sample material (~2 mg) was resuspended in ethanol (~30 μL, Merck) and pipetted onto a polished silicon wafer (Sil'tronix Silicon Technologies, France). All Fe(II)-reacted samples were deposited and dried onto the Si wafers under a glovebox atmosphere and were measured within 1 week in ambient air. Samples were analyzed in Bragg–Brentano geometry using Cu Kα radiation (λ = 1.5418 Å, 40 kV, and 40 mA) and a high-resolution energy-dispersive 1D detector (LYNXEYE). Diffractograms were

DOI: 10.1021/acs.est.8b03206
Environ. Sci. Technol. 2018, 52, 12316–12326

recorded from 10−70° 2θ with a step size of 0.02° 2θ and a 10 s acquisition time per step. The relative contributions of mineral phases in diffraction patterns was determined by Rietveld quantitative phase analysis (QPA) with Fh included as a mass-calibrated PONKCS phase. All calculations were performed in TOPAS software (Version 5, Bruker AXS). Further details and a discussion of the validity of these analyses are found in the Supporting Information.

^{57}Iron Mössbauer Spectroscopy. Mössbauer spectra of selected samples were obtained with a ^{57}Co/Rh γ-radiation source with an activity of ∼20 mCi vibrated in a constant acceleration mode in a standard setup (WissEl, Wissenschaftliche Elektronik GmbH). Sample material (30−60 mg) was loaded into Plexiglas sample holders (∼1 cm^2) in a glovebox (100% N_2) under anoxic conditions. All samples were mounted in transmission geometry. Sample temperatures were maintained with a closed-cycle cryostat (SHI-850-I, Janis Research Co.), whereas the ^{57}Co/Rh source remained at room temperature. Spectra were collected at 5 K and analyzed using the Recoil software (University of Ottawa, Canada) by applying an extended Voigt-based fitting routine.[56] The spectra were calibrated against 7 μm thick α-^{57}Fe^0 at 295 K, and center shifts (CS) are quoted relative to this. For all samples, the half width at half-maximum was fixed to 0.13 mm/s; the value of the inner line broadening of the calibration foil at 295 K.

RESULTS AND DISCUSSION

Total Aqueous Concentrations and Fe_{aq} Speciation. Dissolved Fe (Fe_{aq}) concentrations relative to the initial aqueous Fe(II) spike (C/C_0) are shown in Figures 1A,B and S5. Absolute Fe_{aq} concentrations including Fe_{aq} speciation data are presented in Figures S6−S8 and show that Fe(II) constituted the vast majority of total Fe_{aq}. For some samples, slight differences between aqueous Fe(II) and total Fe_{aq} may result from organically complexed Fe(III) formed during dissolution and reprecipitation of secondary mineral phases or readily reducible Fe(III) oxyhydroxide colloids.[57] However, in future references, "Fe_{aq}" is assumed to comprise aqueous Fe(II). Within the first 6 h of reaction, each treatment showed a drop in Fe_{aq} concentrations (Figures 1A,B and S5), indicating that Fe(II) adsorbed onto the coprecipitate surface[28,31,34,47] or was incorporated into the solid-phase.[58,59] After 24 h, Fe_{aq} concentrations in the coprecipitates stabilized except for suspensions in which magnetite formation further consumed Fe_{aq} (cp. Figures 1, 3, S5, and S11). For Floc 5S, increasing Fe_{aq} concentrations after 2 weeks may be attributed to the poorly crystalline nature of floc Fe minerals[6,34,51] or the release of small contributions from OM-complexed Fe(II/III)[6] during Fe(II)-induced disaggregation (Figure S5). However, this could not be confirmed due to the use of the organic MOPS buffer. Nevertheless, minimal change in solid-phase C content of Fe(II)-reacted samples indicated that no treatment resulted in the significant release of C to solution (Table S1), although rapid de- and re-adsorption cannot be excluded. Aqueous Fe concentrations in Fe(II)-free controls remained below 0.05 mM, implying negligible contributions from microbial activity.

Because Fe(II)-catalyzed mineral transformations may impact trace metal(loid) partitioning on Fe(III) (oxyhydr)oxides[52,60−64] and Floc 5S naturally contained 1.28 mg/g As (Table S1),[34,51] As_{aq} was additionally quantified in Floc 5S treatments. However, in agreement with previous work, no release of As was recorded over the duration of the experiment (Figure S9), despite exposure to significantly higher Fe(II):Fe(III) ratios (0.007 and 0.072 in ref 34 vs 0.05−0.5 in the current study). This may indicate the structural incorporation of As into secondary Fe(III) (oxyhydr)oxides,[52] minimal mineral transformation,[34] or the rapid de- and re-adsorption of As.

Trends in the Fe Isotope Composition of Fe_{aq}. Adsorption or structural incorporation of Fe(II) added with the ^{57}Fe-enriched spike, as described in the previous section, would not result in a change in the fraction of ^{57}Fe in solution ($f^{57}Fe_{aq}$); only $f^{57}Fe$ of the solid phase would increase. However, in all experiments, we observed a rapid drop in $f^{57}Fe_{aq}$, documenting the release of structural Fe(III) via atom exchange between the solution and solid phase Fe. Temporal changes in the Fe_{aq} isotope composition are presented in Figures 1C,D and S5D−F, and the data are further summarized in Tables S4−S6. The most significant alterations in $f^{57}Fe_{aq}$ occurred during the first week, after which values stabilized. For the pure Fh, $f^{57}Fe_{aq}$ reached minima of 3.81, 5.79, and 23.32%; well below the isotopic composition of the total system for aqueous ^{57}Fe(II) additions of 0.5, 1.0, and 5.0 mM, respectively (Figures 1C,D and S5E, Table S3). A $f^{57}Fe_{aq}$ lower than the total system effectively implies that ^{57}Fe is enriched in the solid-phase in relation to the system. This may result from the adsorption of ^{57}Fe(II) onto the solid-phase followed by the immediate oxidation and precipitation of comparatively more crystalline Fe minerals like lepidocrocite, goethite, or magnetite.[28,30−32,34] The Fe(II)-catalyzed mineral transformation or recrystallization of lepidocrocite and goethite proceeds on time scales of days to months;[26,27,31] significantly slower than that of Fh (hours).[28,30−32] Therefore, it is plausible that the ^{57}Fe(II) adsorbs, oxidizes, and precipitates as a crystalline Fe mineral, becoming effectively "locked-up" in the solid-phase, while the Fe(II)-catalyzed transformation of the poorly crystalline Fh continues, resulting in the continual release of structural Fh−Fe (largely ^{56}Fe) and low $f^{57}Fe$ in solution. Selective reduction of Fh may continue until (i) Fh is no longer available or (ii) time scales are reached in which Fe(II)-catalyzed mineral transformations of the ^{57}Fe-enriched crystalline minerals (e.g., lepidocrocite) could be expected, thereby releasing ^{57}Fe back to solution. The latter could explain the subsequent increase in $f^{57}Fe_{aq}$ after 24 h in Fh treatments with the lower aqueous Fe(II) additions (0.5 and 1.0 mM, Figures 1C and S5E). In contrast, with 5 mM Fe(II), low $f^{57}Fe_{aq}$ are maintained for the duration of the experiment. Considering the mmol $Fe(II)_{spike}$:g Fh ratio (∼5, Table S2) and the near complete absence of Fe_{aq} after 72 h (Figure 1B), the residually low $f^{57}Fe_{aq}$ for this sample likely indicates Fe(II) incorporation into the solid-phase and magnetite growth (Figure 3).[30]

Of the Fh−OM coprecipitates, Fh−PGA_0.05 was most similar to the pure Fh, though with slightly higher $f^{57}Fe_{aq}$ minima (4.64, 6.19, and 23.93% for 0.5, 1.0, and 5.0 mM Fe(II), respectively, Figures 1C,D and S5E). For the remaining coprecipitates (Fh−PGA_0.7, Fh−PGA_1.2, and Fh−PGA_2.5), changes to $f^{57}Fe_{aq}$ were comparatively slower for all Fe(II) additions (Figures 1C,D and S5). However, at 5 weeks, $f^{57}Fe_{aq}$ in these samples approached the isotopic composition of the system. Moreover, the isotope composition of the final solid-phases also approached that of the system (Figures 1C,D and S5D−F), indicating a high degree of iron atom exchange. In contrast, solution data for Floc 5S indicated the least change in $f^{57}Fe$ at all $Fe(II)_{spike}$ concentrations (Figure S5). Inhibited iron atom exchange in Floc 5S may result from

DOI: 10.1021/acs.est.8b03206
Environ. Sci. Technol. 2018, 52, 12316−12326

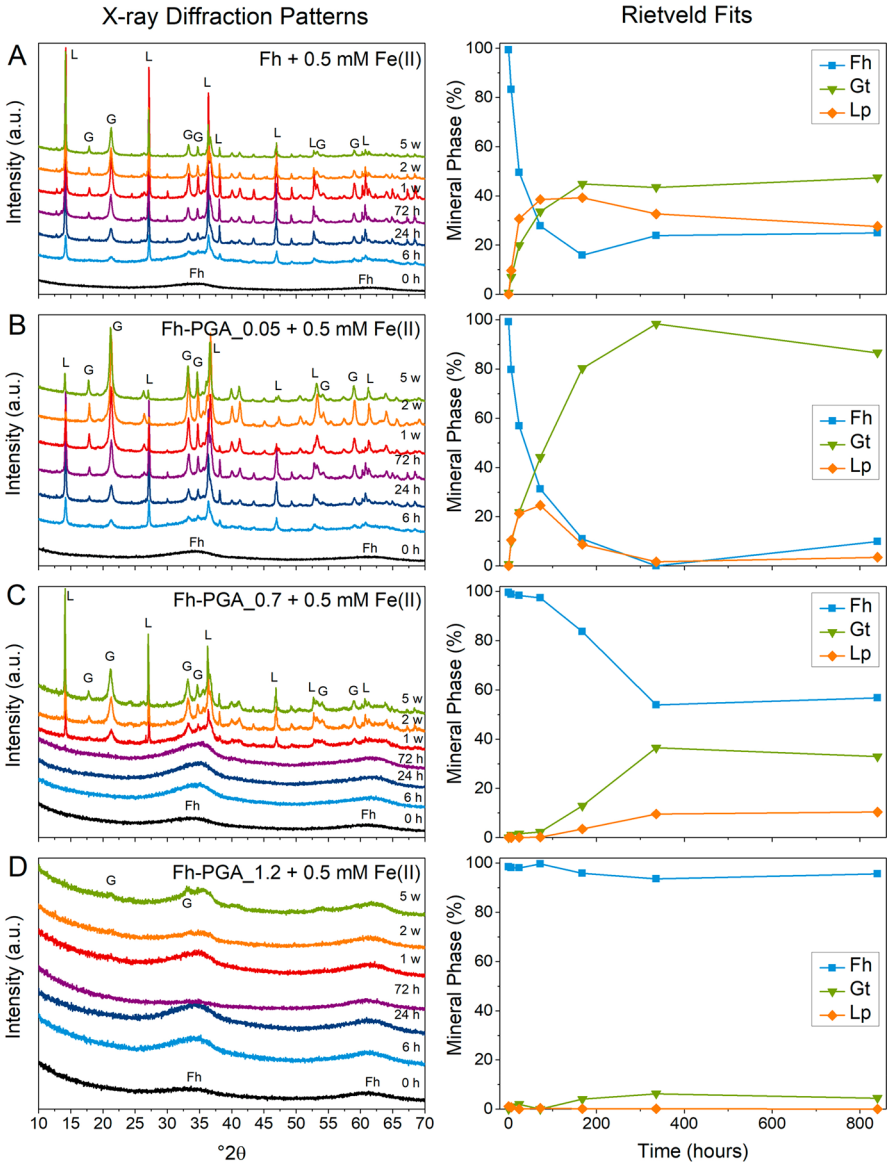

Figure 2. (Left panels) X-ray diffraction patterns of samples prior to and during reaction with 0.5 mM Fe(II), and (right panels) corresponding mineral phase contributions determined with Rietveld QPA, whereby Fh was treated as a PONKCS phase. Abbreviations: h = hours, w = weeks, Fh = ferrihydrite, G/Gt = goethite, L/Lp = lepidocrocite, and PGA = polygalacturonic acid. Additional XRD patterns and corresponding Rietveld fits are presented in the Supporting Information, Figures S10−S13.

an abundance of natural OM or other stabilizing components (e.g., As,[53] Si[37]) in flocs,[6,34] or it reflects the slower Fe(II)-catalyzed reduction kinetics of lepidocrocite,[31] of which Floc 5S Fe minerals contain ∼50%.[34,51]

Solid-Phase Mineral Analyses: X-ray Diffraction. The quantitative interpretation of XRD patterns of samples containing 2-line Fh together with more crystalline iron (oxyhydr)oxide minerals using the PONKCS method in Rietveld analysis has been tested here for the first time. The validity of this approach was tested by analyzing physical mixtures of Fh and goethite, which were prepared, measured, and fitted in a manner identical to the ^{57}Fe(II) experimental samples (Figure S1). The fitting results demonstrate that the quantification of Fh in mixtures is valid; however, they have a larger relative uncertainty at low Fh contents (Figure S2). Examples for Rietveld fits using the PONKCS method applied to selected samples from the mineral transformation experiments are presented in Figure S4.

X-ray diffraction patterns and their corresponding Rietveld results illustrate the temporal evolution of mineral phase transformations in Fe(II)-reacted coprecipitates and Floc 5S in Figures 2, 3, and S10−S13. Detailed fit parameters are presented in Tables S7−S9. At all $Fe(II)_{spike}$ concentrations, mineral transformations are most pronounced for the pure Fh, where rapid formation of crystalline mineral phases coincides with dramatic decreases in Fh contributions within the first 24 h (Figures 2A, 3A, and S11A). Thereafter, at low $Fe(II)_{spike}$ concentrations (0.5 and 1.0 mM Fe(II)) goethite precipitation continues, while magnetite accumulates at the higher $Fe(II)_{spike}$ concentration. Both minerals appear to grow at the expense of lepidocrocite, consistent with previous studies suggesting lepidocrocite to be an intermediary phase.[28,30,65] The rapid precipitation and subsequent dissolution of lepidocrocite agrees well with concomitant trends in $f^{57}Fe_{aq}$ (Figures 1C,D and S5E), confirming that the adsorbed ^{57}Fe(II) rapidly oxidized to form ^{57}Fe-enriched lepidocrocite and goethite.

DOI: 10.1021/acs.est.8b03206
Environ. Sci. Technol. 2018, 52, 12316−12326

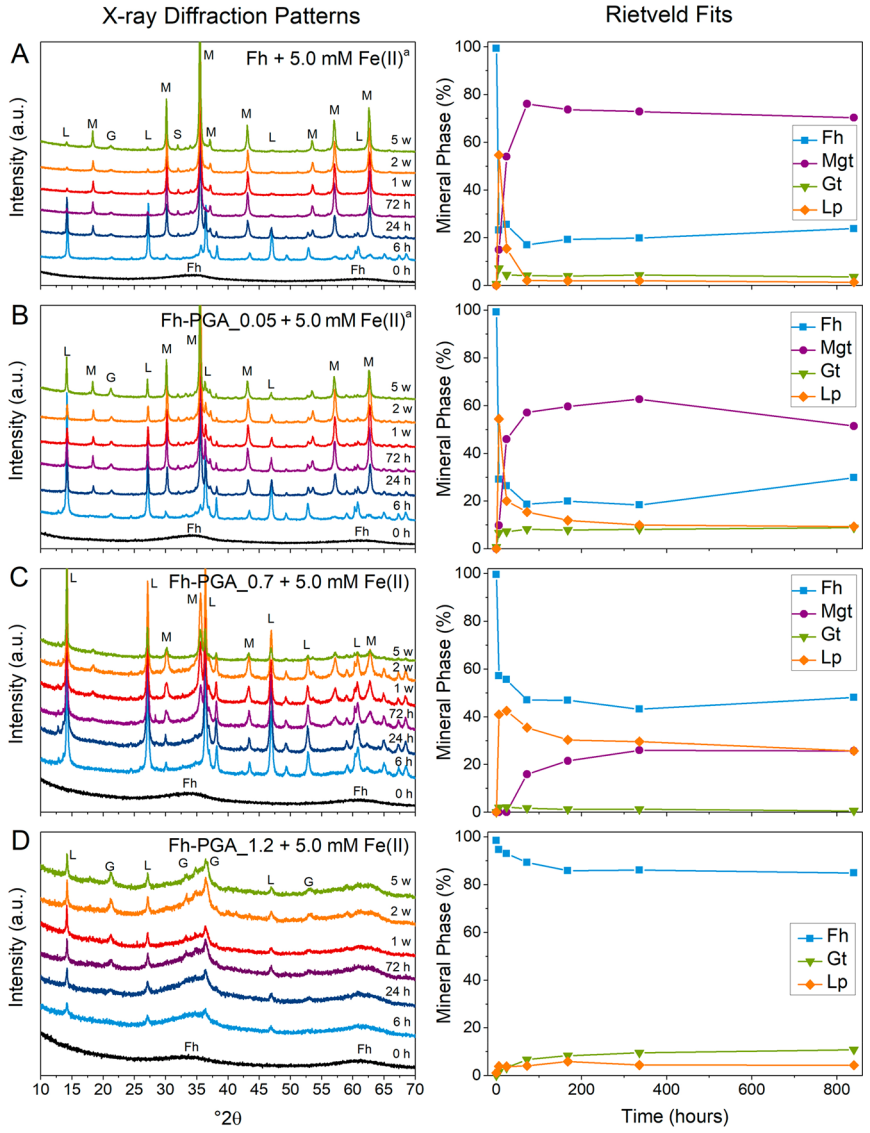

Figure 3. (Left panels) X-ray diffraction patterns of samples prior to and during reaction with 5.0 mM Fe(II), and (right panels) corresponding mineral phase contributions determined with Rietveld QPA, whereby Fh was treated as a PONKCS phase. Abbreviations: h = hours, w = weeks, Fh = ferrihydrite, G/Gt = goethite, L/Lp = lepidocrocite, PGA = polygalacturonic acid, and S = siderite. [a]Samples contained ≤1.5% siderite (contribution not shown in Rietveld fit). Additional XRD patterns and corresponding Rietveld fits are presented in the Supporting Information, Figures S10–S13.

Comparing pure Fh treatments to low C content coprecipitates highlights the influence OM exerts on secondary mineral formation pathways. For Fh–PGA_0.05 reacted with 0.5 and 1.0 mM Fe(II), goethite dominated secondary mineral formation; far exceeding the goethite contributions in the pure Fh treatments (cp. panels E and F in Figures 2 and S5). Enhanced goethite precipitation is expected with higher concentrations of solid-phase-associated Fe(II),[28] suggesting that the presence of low amounts of OM in Fh–PGA_0.05 significantly altered the surface of the coprecipitated Fh; leading to locally high concentrations of solid-phase-associated Fe(II) and thus localized goethite precipitation. Alternatively, analyses of the lepidocrocite crystallite size fitted during Rietveld QPA suggests that low concentrations of OM may inhibit lepidocrocite crystal growth. During the first 72 h, lepidocrocite crystallite size in 0.5 and 1.0 mM Fe(II)-reacted Fh–PGA_0.05 was up to 34% smaller than in the pure Fh (Table S10). Smaller lepidocrocite crystallite size may accelerate reactions with aqueous Fe(II),[31] subsequently promoting its transformation to goethite.

With increasing C content of the coprecipitates, formation of stable crystalline mineral phases was synchronously inhibited. At lower $Fe(II)_{spike}$ concentrations (0.5 and 1.0 mM Fe(II)), goethite contributions at 5 weeks were reduced by 5–7% between Fh–PGA_0.05 and Fh–PGA_1.2, while at higher $Fe(II)_{spike}$ concentrations (1.0 and 5.0 mM Fe(II)), the presence of OM hindered magnetite precipitation. After 24 h, magnetite accounted for 73 ± 2, 58 ± 5, and 22 ± 5% of solid-phase minerals in Fh, Fh–PGA_0.05, and Fh–PGA_0.7 reacted with 5.0 mM Fe(II), respectively (Figure 3, Table S9). Despite the addition of sufficient Fe(II) to convert all Fh to stoichiometric magnetite (Table S2), incomplete conversion may be a reflection of the experimental pH of 7,[30] or indicate the accumulation of Fe(II) on the surface, which may render the electron transfer less energetically favorable.[66] For treatments with OM, incomplete conversion may be an effect

DOI: 10.1021/acs.est.8b03206
Environ. Sci. Technol. 2018, 52, 12316–12326

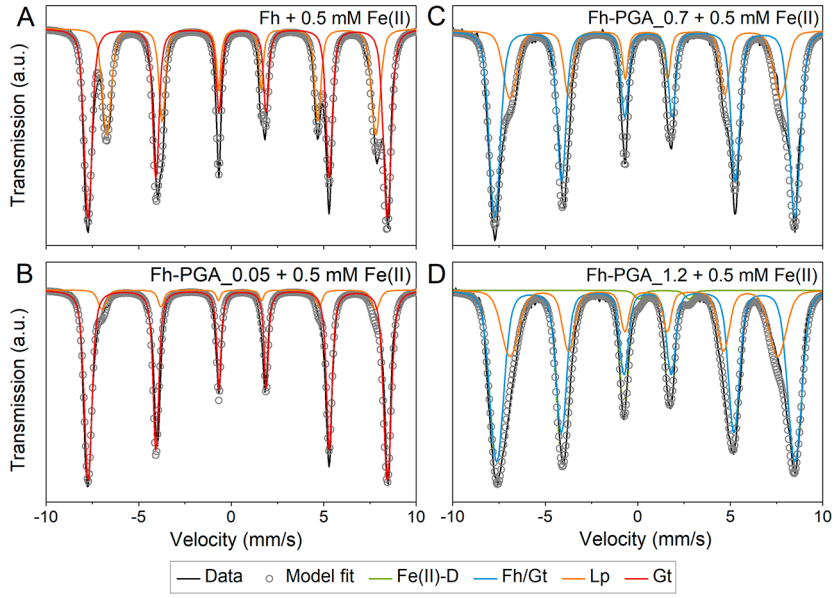

Figure 4. The 5 K Mössbauer spectra of selected samples reacted with 0.5 mM Fe(II) . Corresponding fit parameters are summarized in Table 1. Additional spectra and fit parameters are presented in the Supporting Information, Figures S16, S17, and S18 and Table S11. Abbreviations: Fe(II)-D = adsorbed Fe(II), Fh = ferrihydrite, Fh/Gt = mixed ferrihydrite and goethite, Lp = lepidocrocite, Gt = goethite, and PGA = polygalacturonic acid.

Table 1. 5 K Mössbauer Parameters of Select Samples Reacted with 0.5 mM Fe(II)

sample	treatment	species	CS[a] (mm/s)	ΔE_Q[b] (mm/s)	ϵ[c] (mm/s)	$\langle\|H\|\rangle$[d] (T)	population[e] (%)
Fh	initial[f]	Fh	0.46		−0.03	48.4	100.0
	0.5 mM Fe(II)	Gt	0.48		−0.13	50.1	61.6 ± 0.2
		Lp	0.51		0.03	45.1	38.5 ± 0.2
Fh−PGA_0.05	initial[g]	Fh					100.0
	0.5 mM Fe(II)	Gt	0.48		−0.13	50.2	90.2 ± 0.3
		Lp	0.45		−0.03	45.8	9.8 ± 0.3
Fh−PGA_0.7	initial[g]	Fh					100.0
	0.5 mM Fe(II)	Lp	0.44		−0.04	45.3	30.4 ± 0.9
		Fh/Gt	0.48		−0.10	50.3	69.6 ± 0.9
Fh−PGA_1.2	initial[g]	Fh					100.0
	0.5 mM Fe(II)	Fe(II)-D	1.41	2.72			1.1 ± 0.2
		Fh/Gt	0.48		−0.05	50.0	67.7 ± 1.3
		Lp	0.39		−0.06	44.9	31.2 ± 1.3

[a]CS with respect to α-^{57}Fe^0. [b]Quadrupole splitting. [c]Quadrupole shift (ϵ = $\Delta E_Q/2$). [d]Mean hyperfine field. [e]Spectral contribution and corresponding fit error. [f]Samples were previously measured and published.[34] [g]Due to identical XRD spectra (Figure S3) and synthesis methods, these samples were assumed to also consist of Fh. Abbreviations: Fh = ferrihydrite, Fh/Gt = mixed ferrihydrite and goethite, Gt = goethite, Lp = lepidocrocite, Fe(II)-D = adsorbed Fe(II), and PGA = polygalacturonic acid. An additional table of fitted Mössbauer parameters is found in the Supporting Information, Table S11.

of coprecipitated OM. Solid-state conversion of Fh via adsorbed Fe(II) into magnetite is expected to occur via nucleation and crystal growth;[67] both mechanisms may be impeded by the increasing presence of solid-associated OM. Additionally, Fe(II) interaction with the organic fraction rather than with the mineral surface, i.e., complexation of Fe(II) by functional groups of solid-associated OM, may have removed Fe(II) from solution without initiating electron transfer, thus lowering the effective Fe(II):Fe(III) molar ratio.

Above a C:Fe molar ratio of 0.7, crystalline mineral phases were either considered minor species (<10%) or were not detectable. Recently, Chen et al.[36] studied the stabilization of Fh by OM during exposure to aqueous Fe(II), finding that the extent of Fe mineral transformation was linearly correlated to increasing C:Fe molar ratios, and that above C:Fe = 1.6, no mineral transformations could be expected. Analysis of the residual Fh fraction in XRD patterns in our samples at 5 weeks showed similar linear correlations (r^2 = 0.979 ± 0.006) and minimal differences between residual Fh in Fh−PGA_1.2 and Fh−PGA_2.5 (Figure S14). However, the slope of the fitted trend line decreases with increasing Fe(II) additions (−27% between 0.5 and 5.0 mM Fe(II)), suggesting that with higher $Fe(II)_{spike}$ concentrations and longer experiment durations, materials with C:Fe molar ratios >1.6 may also undergo mineral transformations.

Solid-Phase Mineral Analyses: ^{57}Fe Mössbauer Spectroscopy. 5K Mössbauer spectra of selected samples reacted with 0.5 mM Fe(II) are shown in Figure 4, and the corresponding fit parameters are presented in Table 1. Additional Mössbauer spectra and fit parameters are found in the Supporting Information. Consistent with XRD data, both Fh and Fh−PGA_0.05 showed nearly complete mineral

DOI: 10.1021/acs.est.8b03206
Environ. Sci. Technol. 2018, 52, 12316−12326

transformation to lepidocrocite and goethite. Above a C:Fe molar ratio of 0.05, all Mössbauer spectra were fitted with a mixed "Fh/Gt" phase (24−70% of Fe_{solid}, Figures 4 and S16−S18), which could not be conclusively defined as either Fh or goethite but had quadrupole shifts (ε) between these respective end members. Irrespective of the $Fe(II)_{spike}$ concentration, the ε of this Fh/Gt phase increasingly resembled Fh with higher coprecipitate−OM contents (Tables 1 and S11). Treatments with 5 mM Fe(II) resulted in significant magnetite precipitation (Figure 3). Owing to the complexity of the magnetite Mössbauer spectrum at liquid helium temperatures,[68,69] these samples could not be fitted unambiguously, and thus Fh, Fh−PGA_0.05, and Fh−PGA_0.7 are shown only as measured data in the Supporting Information (Figure S18).

In contrast to XRD, which only detects phases with some degree of crystallinity, Mössbauer spectroscopy is sensitive to atomic nuclei capable of recoilless absorption and emission of γ-radiation; i.e., in our case, every type of solid containing structural or adsorbed ^{57}Fe. Although all initial solids contained a natural-abundance Fe ($f^{57}Fe$ = ∼2.12%), the $^{57}Fe(II)$ spikes resulted in $^{57}Fe(II)_{spike}$:$^{57}Fe_{native}$ ratios of 2.24−22.41 (Table S2), meaning that Mössbauer spectra of Fe(II)-reacted samples are strongly dominated by Fe atoms originating from the $^{57}Fe(II)$ spike. For these reasons, XRD and Mössbauer results are considered complementary rather than comparative, with each method addressing individual aspects of the solid-phase. The ability to quantify solid-associated Fe(II) via Mössbauer spectroscopy is particularly advantageous to this study. Indeed, in samples with C:Fe molar ratios >0.7, spectral contributions from solid-associated Fe(II) increased with both higher $Fe(II)_{spike}$ concentrations as well as OM content, accounting for up to 9.7% of solid-phase Fe (Fe(II)-D, Tables 1 and S11). These data complement the observed trends in Fe_{aq}, where higher removal of Fe_{aq} from solution was recorded in Fh−PGA_2.5 than in Fh−PGA_1.2 reacted with 1.0 and 5.0 mM Fe(II) (cp. Figures 1B and S5B,C). In agreement with previous work,[34] the CS and quadrupole shift (ε) of the Fe(II)-phase did not match typical values of common Fe(II) minerals, like green rust ($[Fe(II)_{(1-n)}Fe(III)_n(OH)_2]^{n+}(CO_3,Cl,SO_4)^{n-}$)[49] or siderite ($FeCO_3$),[48] or Fe(II) adsorbed onto mineral surfaces.[47] Increasing solid-associated Fe(II) contributions with higher OM loadings and $Fe(II)_{spike}$ concentrations and the absence of solid-associated Fe(II) in Fh, Fh−PGA_0.05, or Fh−PGA_0.7, samples reacted with 0.5 or 1.0 mM Fe(II) further support the argument that Fe(II) is likely complexed by excess carboxyl groups (PGA) or carboxy-phenolic moieties (Floc 5S) in the OM.

As discussed above, XRD and Mössbauer results are not directly comparable. However, for coprecipitates with C:Fe molar ratios >0.7 (>1.2 for reactions with 5.0 mM Fe(II)), Mössbauer detection of significant contributions of lepidocrocite (up to 39% of solid-phase Fe) in the absence of any diffraction peak is noteworthy (e.g., cp. Figures 2D and 4D). As even nanometer-sized lepidocrocite may appear as broad reflections in XRD spectra[6,34] (see Floc 5S, Figure S10A), it is plausible that the lepidocrocite detected via Mössbauer in these samples consists of X-ray amorphous clusters.[70] To confirm the presence of lepidocrocite, fits containing a singular Fh/Gt phase were tested with and without the addition of a second sextet (Figure S19). For all spectra, inclusion of a second sextet with parameters similar to lepidocrocite resulted in improved model fits, and therefore lepidocrocite was included. For Fe(II)-reacted Floc 5S, the lepidocrocite fraction similarly increases (from 33 to 69 ± 7%, Table S11); however, floc-lepidocrocite is initially nanocrystalline,[6,34,51] thus it is not possible to determine if Fe(II)-reacted Floc 5S contained additional nanocrystalline lepidocrocite.

Fate of the Added Fe(II) and the Impact of Increasing OM Content. By using stable Fe isotopes as tracers and following temporal changes in solid-phase mineral compositions, we were able to document that, in reactions between aqueous $^{57}Fe(II)$ and poorly crystalline Fh with low OM content (C:Fe molar ratio ≤0.05), adsorbed Fe(II) immediately oxidizes to precipitate crystalline ^{57}Fe-enriched mineral phases, effectively "locking-up" the added $^{57}Fe(II)$ while the preferential reduction of poorly crystalline Fh (^{56}Fe) continues, resulting in $f^{57}Fe_{aq}$ values lower than those of the total system. In contrast, in Fh−PGA coprecipitates with C:Fe molar ratios ≥0.7, the presence of OM inhibits the formation of ^{57}Fe-enriched crystalline minerals, forming instead new poorly crystalline minerals which react similarly fast with the remaining aqueous Fe(II) compared to the initial Fh. In addition, complexation of $^{57}Fe(II)$ by organic functional groups, as seen in the increasing fractions of solid-associated Fe(II) with increasing Fe(II) and OM content, results in the removal of aqueous Fe(II) from solution without changing $f^{57}Fe_{aq}$. These factors combine to explain why trends in Fe_{aq} and the fraction of ^{57}Fe in solution do not follow trends in increasing C:Fe molar ratios (Figures 1 and S5).

Congruent increases in $Fe(II)_{spike}$ concentrations and C content of Fh−OM coprecipitates permit an examination of their competing effects. Higher $Fe(II)_{spike}$ concentrations are expected to result in faster mineral transformations.[30] Indeed, for pure Fh reacted with 0.5, 1.0, and 5.0 mM Fe(II), the remaining Fh fraction after 6 h of reaction decreases from 83 to 54 to 23%, respectively, for an average of −46 ± 17% with each increase in $Fe(II)_{spike}$ concentration (Figures 2A, 3A, and S11A). For Fh−PGA_0.05 and Fh−PGA_0.7, the average differences drop to −36 ± 32 and −21 ± 28%, respectively, and above a C:Fe molar ratio of 0.7, less than −2% change in crystalline solid-phase mineral contribution is recorded within 6 h (Figures 2, 3, and S10−S13). Therefore, at lower C:Fe molar ratios (≤0.7), it appears that transformation kinetics are dictated by $Fe(II)_{spike}$ concentrations, while at higher C loadings, OM content dictates transformation kinetics irrespective of Fe(II) present.

Mechanisms Involved in the Effect of OM. Our results on Fe(II)-catalyzed mineral transformation and iron atom exchange with pure Fh and Fh−PGA coprecipitates, in which we varied the C:Fe ratio as well as the added $Fe(II)_{spike}$ concentration, allow us to constrain the possible mechanisms of how OM affects the formation of more crystalline iron minerals. Possible mechanisms discussed in previous studies include the complexation of Fe(II) by the OM, removing aqueous Fe(II) from solution without initiating atom exchange, and mineral transformations.[34,36] Another contributing factor may be the blockage of mineral surface sites or micropore entrances by coprecipitated OM, hindering aqueous Fe(II) from adsorbing to and transferring an electron to the Fh structure.[12,34] However, our results clearly demonstrated that iron atom exchange between aqueous Fe(II) and Fe in Fh−PGA coprecipitates is fast and nearly complete within 168 h, even at high C:Fe ratios. The amounts of Fe_{aq} removed within the first 6 h after the $^{57}Fe(II)$ spike suggested that the PGA

DOI: 10.1021/acs.est.8b03206
Environ. Sci. Technol. 2018, 52, 12316−12326

contributed little to the overall adsorption of Fe(II), and that most Fe(II) was adsorbed to the Fh in coprecipitates (Figure S20). This seems plausible, since Fe(II) is strongly adsorbed to Fe(III) oxyhydroxide surfaces at pH 7.[47] Further, our results show that despite rapid iron atom exchange, which also implies electron transfer between adsorbed Fe(II) and structural Fe(III), no formation of crystalline iron minerals was detectable by X-ray diffraction. However, analysis of the final solids by Mössbauer spectroscopy suggested that nanosized clusters with lepidocrocite (and possibly goethite) structure may have formed but were still undistinguishable from Fh by XRD. On the basis of these results, we conclude that the effects of OM on Fe(II)-catalyzed transformation of Fh cannot be explained by surface or pore blocking. Instead, we postulate that OM hinders crystal growth of goethite, lepidocrocite, and magnetite, so that the newly formed materials are again Fh or nanoclusters of the lepidocrocite-like structure. The transformation of Fh to crystalline goethite during aging at elevated temperatures can occur via oriented aggregation growth, whereby nanosized clusters of goethite aggregate in an oriented fashion and subsequently form an acicular goethite.[71,72] Oriented aggregation growth was also reported to be important in the Fe(II)-catalyzed transformation of lepidocrocite to goethite at a low temperature, in addition to the classical dissolution-reprecipitation mechanism.[73] Oriented aggregation growth is favored by pH values close to the point-of-zero-charge (PZC) of the clusters, which is the case in our experiments (pH 7). The addition of OM, such as PGA, renders the surface charge negative[74] and may thereby hinder oriented aggregation growth. Additionally, surface interactions with macromolecular OM may sterically hinder the free movement and alignment of nanoclusters and inhibit attachment and formation of larger crystals. Adsorbed OM may also poison crystal growth of lepidocrocite, goethite, and magnetite during dissolution-reprecipitation processes.

Environmental Implications. With the addition of aqueous Fe(II) at circum-neutral pH, the shift from X-ray amorphous Fh to a crystalline Fe mineral-dominated system occurs rapidly (<24 h) in the presence of low or no OM, with the OM content strongly influencing mineral transformation end-products. Therefore, in mineral subsoil horizons or mining-derived mineral substrates, where C:Fe molar ratios are often low compared to the coprecipitates in this study, even short-term fluctuations in the prevailing redox conditions may significantly impact the biogeochemical cycling of contaminants and nutrients by changing the sorption capacities of mineral phases. In contrast, in organic-rich surface soils, marine sediments, and wetlands, or where Fe(III) (oxyhydr)oxide formation may be biotically driven (i.e., freshwater flocs), C:Fe molar ratios may reach higher values (>0.7). Here, prolonged exposure of mineral-organic associations to Fe(II) may have a limited impact on mineral phase crystallinity. However, because the iron atom exchange still occurs, there is still potential for the release or repartitioning of contaminants and nutrients associated with the iron oxides during extended oscillating redox conditions.

■ ASSOCIATED CONTENT

Supporting Information

The Supporting Information is available free of charge on the ACS Publications website at DOI: 10.1021/acs.est.8b03206.

Details to experimental materials and setup, Fe_{aq} speciation, tables of Fe isotope data, and additional XRD and Mössbauer data (PDF)

■ AUTHOR INFORMATION

Corresponding Author

*E-mail: laurel.thomas@usys.ethz.ch.

ORCID

Laurel K. ThomasArrigo: 0000-0002-6758-3760
James M. Byrne: 0000-0002-4399-7336
Andreas Kappler: 0000-0002-3558-9500
Ruben Kretzschmar: 0000-0003-2587-2430

Notes

The authors declare no competing financial interest.

■ ACKNOWLEDGMENTS

We are grateful to K. Barmettler (ETH Zurich) for assisting with laboratory analyses and to C. Mikutta (Leibniz Universität Hannover) for helping with floc sampling at Gola di Lago. This work was funded by ETH Zürich.

■ REFERENCES

(1) Borch, T.; Kretzschmar, R.; Kappler, A.; Van Cappellen, P.; Ginder-Vogel, M.; Voegelin, A.; Campbell, K. Biogeochemical redox processes and their impact on contaminant dynamics. *Environ. Sci. Technol.* **2010**, *44*, 15−23.

(2) Melton, E. D.; Swanner, E. D.; Behrens, S.; Schmidt, C.; Kappler, A. The interplay of microbially mediated and abiotic reactions in the biogeochemical Fe cycle. *Nat. Rev. Microbiol.* **2014**, *12*, 797−808.

(3) Eusterhues, K.; Rumpel, C.; Kögel-Knabner, I. Organo-mineral associations in sandy acid forest soils: importance of specific surface area, iron oxides and micropores. *Eur. J. Soil Sci.* **2005**, *56*, 753−763.

(4) Torn, M. S.; Trumbore, S. E.; Chadwick, O. A.; Vitousek, P. M.; Hendricks, D. M. Mineral control of soil organic carbon storage and turnover. *Nature* **1997**, *389*, 170−173.

(5) Kögel-Knabner, I.; Guggenberger, G.; Kleber, M.; Kandeler, E.; Kalbitz, K.; Scheu, S.; Eusterhues, K.; Leinweber, P. Organo-mineral associations in temperate soils: Integrating biology, mineralogy, and organic matter chemistry. *J. Plant Nutr. Soil Sci.* **2008**, *171*, 61−82.

(6) ThomasArrigo, L. K.; Mikutta, C.; Byrne, J.; Barmettler, K.; Kappler, A.; Kretzschmar, R. Iron and arsenic speciation and distribution in organic flocs from streambeds of an arsenic-enriched peatland. *Environ. Sci. Technol.* **2014**, *48*, 13218−13228.

(7) Lalonde, K.; Mucci, A.; Ouellet, A.; Gélinas, Y. Preservation of organic matter in sediments promoted by iron. *Nature* **2012**, *483*, 198−200.

(8) Plach, J. M.; Elliott, A. V. C.; Droppo, I. G.; Warren, L. A. Physical and ecological controls on freshwater floc trace metal dynamics. *Environ. Sci. Technol.* **2011**, *45*, 2157−2164.

(9) Chan, C. S.; Fakra, S. C.; Edwards, D. C.; Emerson, D.; Banfield, J. F. Iron oxyhydroxide mineralization on microbial extracellular polysaccharides. *Geochim. Cosmochim. Acta* **2009**, *73*, 3807−3818.

(10) Schwertmann, U.; Murad, E. The nature of an iron oxide-organic iron association in a peaty environment. *Clay Miner.* **1988**, *23*, 291−299.

(11) Riedel, T.; Zak, D.; Biester, H.; Dittmar, T. Iron traps terrestrially derived dissolved organic matter at redox interfaces. *Proc. Natl. Acad. Sci. U. S. A.* **2013**, *110*, 10101−10105.

(12) Chen, C. M.; Dynes, J. J.; Wang, J.; Sparks, D. L. Properties of Fe-organic matter associations via coprecipitation versus adsorption. *Environ. Sci. Technol.* **2014**, *48*, 13751−13759.

(13) Du, Y. X.; Ramirez, C. E.; Jaffé, R. Fractionation of dissolved organic matter by co-precipitation with iron: Effects of composition. *Environ. Process.* **2018**, *5*, 5−21.

DOI: 10.1021/acs.est.8b03206
Environ. Sci. Technol. 2018, 52, 12316−12326

(14) Mikutta, C. X-ray absorption spectroscopy study on the effect of hydroxybenzoic acids on the formation and structure of ferrihydrite. *Geochim. Cosmochim. Acta* **2011**, *75*, 5122−5139.
(15) Eusterhues, K.; Wagner, F. E.; Häusler, W.; Hanzlik, M.; Knicker, H.; Totsche, K. U.; Kögel-Knabner, I.; Schwertmann, U. Characterization of ferrihydrite-soil organic matter coprecipitates by X-ray diffraction and Mössbauer spectroscopy. *Environ. Sci. Technol.* **2008**, *42*, 7891−7897.
(16) Schwertmann, U.; Wagner, F.; Knicker, H. Ferrihydrite-humic associations: Magnetic hyperfine interactions. *Soil Sci. Soc. Am. J.* **2005**, *69*, 1009−1015.
(17) Eusterhues, K.; Rennert, T.; Knicker, H.; Kögel-Knabner, I.; Totsche, K. U.; Schwertmann, U. Fractionation of organic matter due to reaction with ferrihydrite: Coprecipitation versus adsorption. *Environ. Sci. Technol.* **2011**, *45*, 527−533.
(18) Posth, N. R.; Huelin, S.; Konhauser, K. O.; Kappler, A. Size, density and composition of cell-mineral aggregates formed during anoxygenic phototrophic Fe(II) oxidation: Impact on modern and ancient environments. *Geochim. Cosmochim. Acta* **2010**, *74*, 3476−3493.
(19) Muehe, E. M.; Scheer, L.; Daus, B.; Kappler, A. Fate of arsenic during microbial reduction of biogenic versus abiogenic As-Fe(III)-mineral coprecipitates. *Environ. Sci. Technol.* **2013**, *47*, 8297−8307.
(20) Larese-Casanova, P.; Haderlein, S. B.; Kappler, A. Biomineralization of lepidocrocite and goethite by nitrate-reducing Fe(II)-oxidizing bacteria: Effect of pH, bicarbonate, phosphate, and humic acids. *Geochim. Cosmochim. Acta* **2010**, *74*, 3721−3734.
(21) Schädler, S.; Burkhardt, C.; Hegler, F.; Straub, K. L.; Miot, J.; Benzerara, K.; Kappler, A. Formation of cell-iron-mineral aggregates by phototrophic and nitrate-reducing anaerobic Fe(II)-oxidizing bacteria. *Geomicrobiol. J.* **2009**, *26*, 93−103.
(22) Lehmann, J.; Kleber, M. The contentious nature of soil organic matter. *Nature* **2015**, *528*, 60−68.
(23) Mikutta, R.; Mikutta, C.; Kalbitz, K.; Scheel, T.; Kaiser, K.; Jahn, R. Biodegradation of forest floor organic matter bound to minerals via different binding mechanisms. *Geochim. Cosmochim. Acta* **2007**, *71*, 2569−2590.
(24) Kaiser, K.; Guggenberger, G. The role of DOM sorption to mineral surfaces in the preservation of organic matter in soils. *Org. Geochem.* **2000**, *31*, 711−725.
(25) Wagai, R.; Mayer, L. M. Sorptive stabilization of organic matter in soils by hydrous iron oxides. *Geochim. Cosmochim. Acta* **2007**, *71*, 25−35.
(26) Handler, R. M.; Beard, B. L.; Johnson, C. M.; Scherer, M. M. Atom exchange between aqueous Fe(II) and goethite: An Fe isotope tracer study. *Environ. Sci. Technol.* **2009**, *43*, 1102−1107.
(27) Handler, R. M.; Frierdich, A. J.; Johnson, C. M.; Rosso, K. M.; Beard, B. L.; Wang, C.; Latta, D. E.; Neumann, A.; Pasakarnis, T.; Premaratne, W. A. P. J.; Scherer, M. M. Fe(II)-catalyzed recrystallization of goethite revisited. *Environ. Sci. Technol.* **2014**, *48*, 11302−11311.
(28) Boland, D.; Collins, R.; Miller, C.; Glover, C.; Waite, T. D. Effect of solution and solid-phase conditions on the Fe(II)-accelerated transformation of ferrihydrite to lepidocrocite and goethite. *Environ. Sci. Technol.* **2014**, *48*, 5477−5485.
(29) Schwertmann, U.; Cornell, R. M. *Iron Oxides in the Laboratory: Preparation and Characterization*; WILEY-VCH Verlag GMBH & Co. KGaA: Weinheim, Germany, 2000.
(30) Hansel, C. M.; Benner, S. G.; Fendorf, S. Competing Fe(II)-induced mineralization pathways of ferrihydrite. *Environ. Sci. Technol.* **2005**, *39*, 7147−7153.
(31) Pedersen, H. D.; Postma, D.; Jakobsen, R.; Larsen, O. Fast transformation of iron oxyhydroxides by the catalytic action of aqueous Fe(II). *Geochim. Cosmochim. Acta* **2005**, *69*, 3967−3977.
(32) Yang, L.; Steefel, C.; Marcus, M. A.; Bargar, J. R. Kinetics of Fe(II)-catalyzed transformation of 6-line ferrihydrite under anaerobic flow conditions. *Environ. Sci. Technol.* **2010**, *44*, 5469−5475.
(33) Jones, A. M.; Collins, R. N.; Waite, T. D. Redox characterization of the Fe(II)-catalyzed transformation of ferrihydrite to goethite. *Geochim. Cosmochim. Acta* **2017**, *218*, 257−272.
(34) ThomasArrigo, L. K.; Mikutta, C.; Byrne, J.; Kappler, A.; Kretzschmar, R. Iron(II)-catalyzed iron atom exchange and mineralogical changes in iron-rich organic freshwater flocs: An iron isotope tracer study. *Environ. Sci. Technol.* **2017**, *51*, 6897−6907.
(35) Liu, H.; Guo, H.; Li, P.; Wei, Y. The transformation of ferrihydrite in the presence of trace Fe(II): The effect of the anionic media. *J. Solid State Chem.* **2008**, *181*, 2666−2671.
(36) Chen, C.; Kukkadapu, R. K.; Sparks, D. L. Influence of coprecipitated organic matter on $Fe^{2+}_{(aq)}$-catalyzed transformation of ferrihydrite: Implications for carbon dynamics. *Environ. Sci. Technol.* **2015**, *49*, 10927−10936.
(37) Jones, A. M.; Collins, R. N.; Rose, J.; Waite, T. D. The effect of silica and natural organic matter on the Fe(II)-catalysed transformation and reactivity of Fe(III) minerals. *Geochim. Cosmochim. Acta* **2009**, *73*, 4409−4422.
(38) Henneberry, Y. K.; Kraus, T. E. C.; Nico, P. S.; Horwath, W. R. Structural stability of coprecipitated natural organic matter and ferric iron under reducing conditions. *Org. Geochem.* **2012**, *48*, 81−89.
(39) Shimizu, M.; Zhou, J.; Schröder, C.; Obst, M.; Kappler, A.; Borch, T. Dissimilatory reduction and transformation of ferrihydrite-humic acid coprecipitates. *Environ. Sci. Technol.* **2013**, *47*, 13375−13384.
(40) Cooper, R. E.; Eusterhues, K.; Wegner, C. E.; Totsche, K. U.; Küsel, K. Ferrihydrite-associated organic matter (OM) stimulates reduction by *Shewanella oneidensis* MR-1 and a complex microbial consortia. *Biogeosciences* **2017**, *14*, 5171−5188.
(41) Mikutta, C.; Kretzschmar, R. Synthetic coprecipitates of exopolysaccharides and ferrihydrite. Part II: Siderophore-promoted dissolution. *Geochim. Cosmochim. Acta* **2008**, *72*, 1128−1142.
(42) Kappler, A.; Benz, M.; Schink, B.; Brune, A. Electron shuttling via humic acids in microbial iron(III) reduction in a freshwater sediment. *FEMS Microbiol. Ecol.* **2004**, *47*, 85−92.
(43) Adhikari, D.; Zhao, Q.; Das, K.; Mejia, J.; Huang, R. X.; Wang, X. L.; Poulson, S. R.; Tang, Y. Z.; Roden, E. E.; Yang, Y. Dynamics of ferrihydrite-bound organic carbon during microbial Fe reduction. *Geochim. Cosmochim. Acta* **2017**, *212*, 221−233.
(44) Pan, W. N.; Kan, J.; Inamdar, S.; Chen, C. M.; Sparks, D. Dissimilatory microbial iron reduction release DOC (dissolved organic carbon) from carbon-ferrihydrite association. *Soil Biol. Biochem.* **2016**, *103*, 232−240.
(45) Daugherty, E. E.; Gilbert, B.; Nico, P. S.; Borch, T. Complexation and redox buffering of iron(II) by dissolved organic matter. *Environ. Sci. Technol.* **2017**, *51*, 11096−11104.
(46) Royer, R. A.; Burgos, W. D.; Fisher, A. S.; Unz, R. F.; Dempsey, B. A. Enhancement of biological reduction of hematite by electron shuttling and Fe(II) complexation. *Environ. Sci. Technol.* **2002**, *36*, 1939−1946.
(47) Williams, A. G. B.; Scherer, M. M. Spectroscopic evidence for Fe(II)-Fe(III) electron transfer at the iron oxide-water interface. *Environ. Sci. Technol.* **2004**, *38*, 4782−4790.
(48) Dyar, M. D.; Agresti, D. G.; Schaefer, M. W.; Grant, C. A.; Sklute, E. C. Mössbauer spectroscopy of earth and planetary materials. *Annu. Rev. Earth Planet. Sci.* **2006**, *34*, 83−125.
(49) Génin, J. M. R.; Bourrie, G.; Trolard, F.; Abdelmoula, M.; Jaffrezic, A.; Refait, P.; Maitre, V.; Humbert, B.; Herbillon, A. Thermodynamic equilibria in aqueous suspensions of synthetic and natural Fe(II)-Fe(III) green rusts: Occurrences of the mineral in hydromorphic soils. *Environ. Sci. Technol.* **1998**, *32*, 1058−1068.
(50) Scarlett, N. V. Y.; Madsen, I. C. Quantification of phases with partial or no known crystal structures. *Powder Diffr.* **2006**, *21*, 278−284.
(51) ThomasArrigo, L. K.; Mikutta, C.; Lohmayer, R.; Planer-Friedrich, B.; Kretzschmar, R. Sulfidization of organic freshwater flocs from a minerotrophic peatland: Speciation changes of iron, sulfur, and arsenic. *Environ. Sci. Technol.* **2016**, *50*, 3607−3616.

DOI: 10.1021/acs.est.8b03206
Environ. Sci. Technol. 2018, 52, 12316−12326

(52) Pedersen, H. D.; Postma, D.; Jakobsen, R. Release of arsenic associated with the reduction and transformation of iron oxides. *Geochim. Cosmochim. Acta* **2006**, *70*, 4116−4129.
(53) Ford, R. G. Rates of hydrous ferric oxide crystallization and the influence on coprecipitated arsenate. *Environ. Sci. Technol.* **2002**, *36*, 2459−2463.
(54) Fortune, W. B.; Mellon, M. G. Determination of iron with *o*-phenanthroline - A spectrophotometric study. *Ind. Eng. Chem., Anal. Ed.* **1938**, *10*, 60−64.
(55) Taylor, P. D. P.; Maeck, R.; Debievre, P. Determination of the absolute isotopic composition and atomic weight of a reference sample of natural iron. *Int. J. Mass Spectrom. Ion Processes* **1992**, *121*, 111−125.
(56) Lagarec, K.; Rancourt, D. G. Extended Voigt-based analytic lineshape method for determining N-dimensional correlated hyperfine parameter distributions in Mossbauer spectroscopy. *Nucl. Instrum. Methods Phys. Res., Sect. B* **1997**, *129*, 266−280.
(57) Tipping, E.; Rey-Castro, C.; Bryan, S. E.; Hamilton-Taylor, J. Al(III) and Fe(III) binding by humic substances in freshwaters, and implications for trace metal speciation. *Geochim. Cosmochim. Acta* **2002**, *66*, 3211−3224.
(58) Tomaszewski, E. J.; Cronk, S. S.; Gorski, C. A.; Ginder-Vogel, M. The role of dissolved Fe(II) concentration in the mineralogical evolution of Fe (hydr)oxides during redox cycling. *Chem. Geol.* **2016**, *438*, 163−170.
(59) Tronc, E.; Belleville, P.; Jolivet, J. P.; Livage, J. Transformation of ferric hydroxide into spinel by Fe(II) adsorption. *Langmuir* **1992**, *8*, 313−319.
(60) Frierdich, A. J.; Catalano, J. G. Controls on Fe(II)-activated trace element release from goethite and hematite. *Environ. Sci. Technol.* **2012**, *46*, 1519−1526.
(61) Jang, J. H.; Dempsey, B. A.; Catchen, G. L.; Burgos, W. D. Effects of Zn(II), Cu(II), Mn(II), Fe(II), NO_3^-, or SO_4^{2-} at pH 6.5 and 8.5 on transformations of hydrous ferric oxide (HFO) as evidenced by Mössbauer spectroscopy. *Colloids Surf., A* **2003**, *221*, 55−68.
(62) Coughlin, B. R.; Stone, A. T. Nonreversible adsorption of divalent metal-ions (Mn^{II}, Co^{II}, Ni^{II}, Cu^{II}, and Pb^{II}) onto goethite: Effects of acidification, Fe^{II} addition, and picolinic acid addition. *Environ. Sci. Technol.* **1995**, *29*, 2445−2455.
(63) Nico, P. S.; Stewart, B. D.; Fendorf, S. Incorporation of oxidized uranium into Fe (hydr)oxides during Fe(II) catalyzed remineralization. *Environ. Sci. Technol.* **2009**, *43*, 7391−7396.
(64) Frierdich, A. J.; Catalano, J. G. Fe(II)-mediated reduction and repartitioning of structurally incorporated Cu, Co, and Mn in iron oxides. *Environ. Sci. Technol.* **2012**, *46*, 11070−11077.
(65) Xiao, W.; Jones, A. M.; Li, X. M.; Collins, R. N.; Waite, T. D. Effect of *Shewanella oneidensis* on the kinetics of Fe(II)-catalyzed transformation of ferrihydrite to crystalline iron oxides. *Environ. Sci. Technol.* **2018**, *52*, 114−123.
(66) Frierdich, A. J.; Helgeson, M.; Liu, C.; Wang, C.; Rosso, K. M.; Scherer, M. M. Iron atom exchange between hematite and aqueous Fe(II). *Environ. Sci. Technol.* **2015**, *49*, 8479−8486.
(67) Hansel, C. M.; Benner, S. G.; Neiss, J.; Dohnalkova, A.; Kukkadapu, R. K.; Fendorf, S. Secondary mineralization pathways induced by dissimilatory iron reduction of ferrihydrite under advective flow. *Geochim. Cosmochim. Acta* **2003**, *67*, 2977−2992.
(68) Harker, S. J.; Pollard, R. J. A study of magentite at 4.2 K and subject to strong applied magnetic fields. *Nucl. Instrum. Methods Phys. Res., Sect. B* **1993**, *76*, 61−63.
(69) Srivastava, C. M.; Shringi, S. N.; Babu, M. V. Mössbauer study of the low-temperature phase of magnetite. *Phys. Status Solidi A* **1981**, *65*, 731−735.
(70) Gebauer, D.; Kellermeier, M.; Gale, J. D.; Bergström, L.; Cölfen, H. Pre-nucleation clusters as solute precursors in crystallisation. *Chem. Soc. Rev.* **2014**, *43*, 2348−2371.
(71) Burleson, D. J.; Penn, R. L. Two-step growth of goethite from ferrihydrite. *Langmuir* **2006**, *22*, 402−409.
(72) Burrows, N. D.; Hale, C. R. H.; Penn, R. L. Effect of pH on the kinetics of crystal growth by oriented aggregation. *Cryst. Growth Des.* **2013**, *13*, 3396−3403.
(73) Yan, W. J.; Liu, H.; Chen, R. F.; Xie, J.; Wei, Y. Dissolution and oriented aggregation: Transformation from lepidocrocite to goethite by the catalysis of aqueous Fe(II). *RSC Adv.* **2015**, *5*, 106396−106399.
(74) Mikutta, C.; Mikutta, R.; Bonneville, S.; Wagner, F.; Voegelin, A.; Christl, I.; Kretzschmar, R. Synthetic coprecipitates of exopolysaccharides and ferrihydrite. Part 1: Characterization. *Geochim. Cosmochim. Acta* **2008**, *72*, 1111−1127.

DOI: 10.1021/acs.est.8b03206
Environ. Sci. Technol. 2018, 52, 12316−12326